Supplement of Atmos. Chem. Phys., 21, 13077–13098, 2021
https://doi.org/10.5194/acp-21-13077-2021-supplement

Atmospheric Chemistry and Physics
Open Access
EGU

Supplement of

Isotopic evidence for dominant secondary production of HONO in near-ground wildfire plumes

Jiajue Chai et al.

Correspondence to: Jiajue Chai (jiajue_chai@brown.edu)

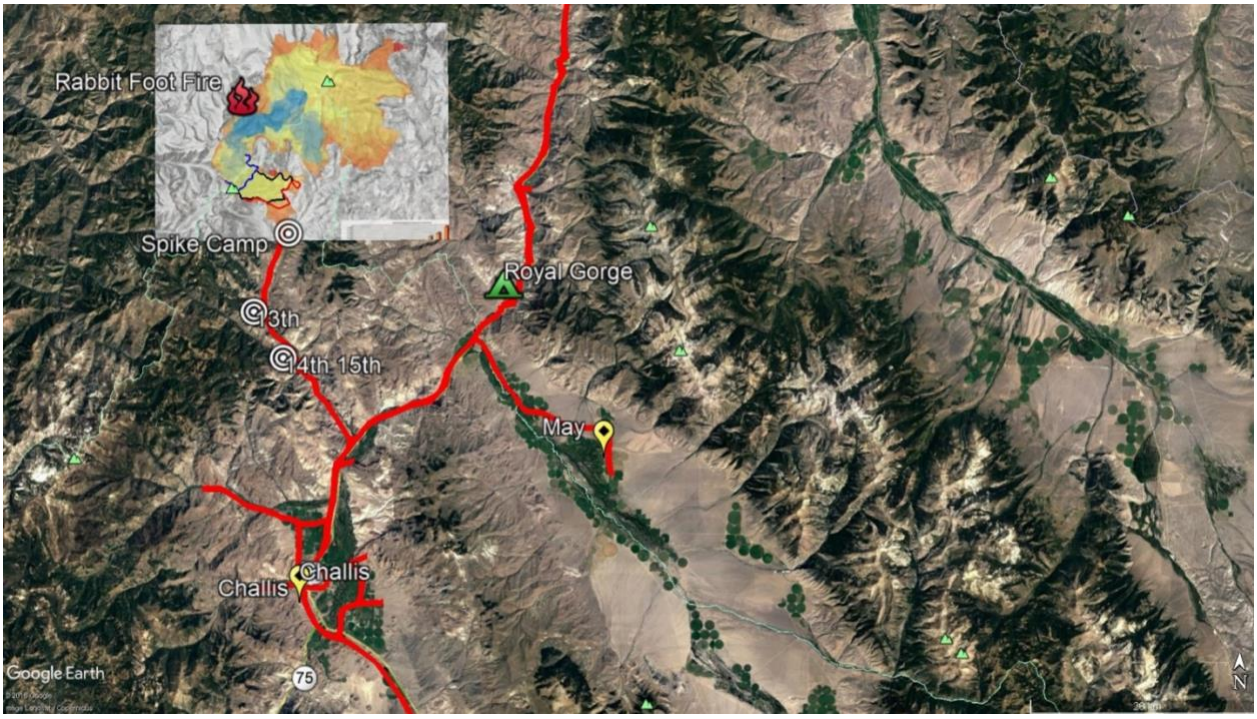

Figure S1. WE-CAN 2018 sampling map for Rabbit Foot fire (RF) in the Challis area of Salmon-Challis National Forest in central Idaho, from August 9th to August 18th 2018. Of note are important dates, which give the locations of the different approaches to the RFF during mobile measurements up MCR (H. Munro, "An Investigation of Nitrous and Nitric Acid Diurnal Cycles in Biomass Burning Plumes", Thesis, University of New Hampshire, Durham, NH, 2019).

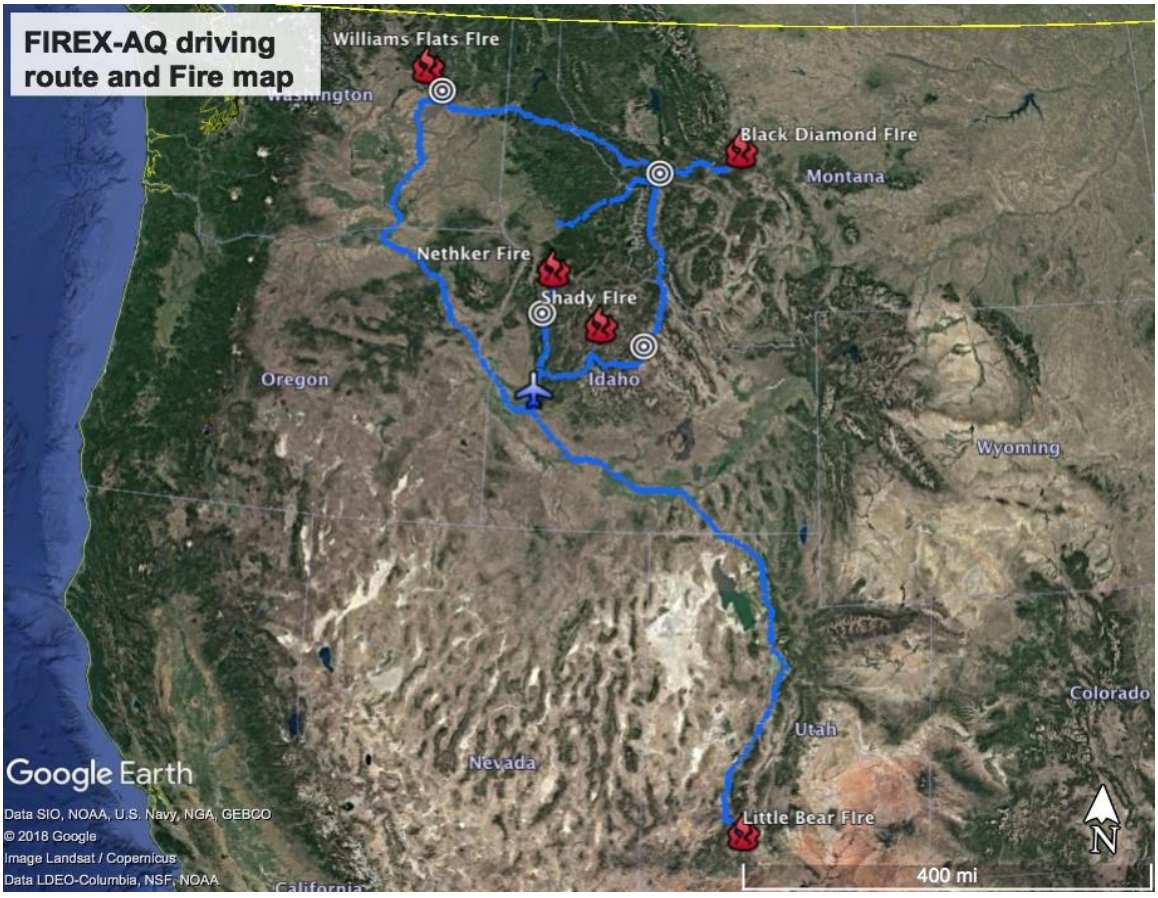

Figure S2. Driving map during FIREX-AQ. From Jul 24 to Aug 22 of 2019, we sampled smoke from five different fires including Shady fire (Idaho), Black Diamond fire (Montana), Williams Flats fire (Washington), Nethker fire (Idaho), and Little Bear fire (Utah).

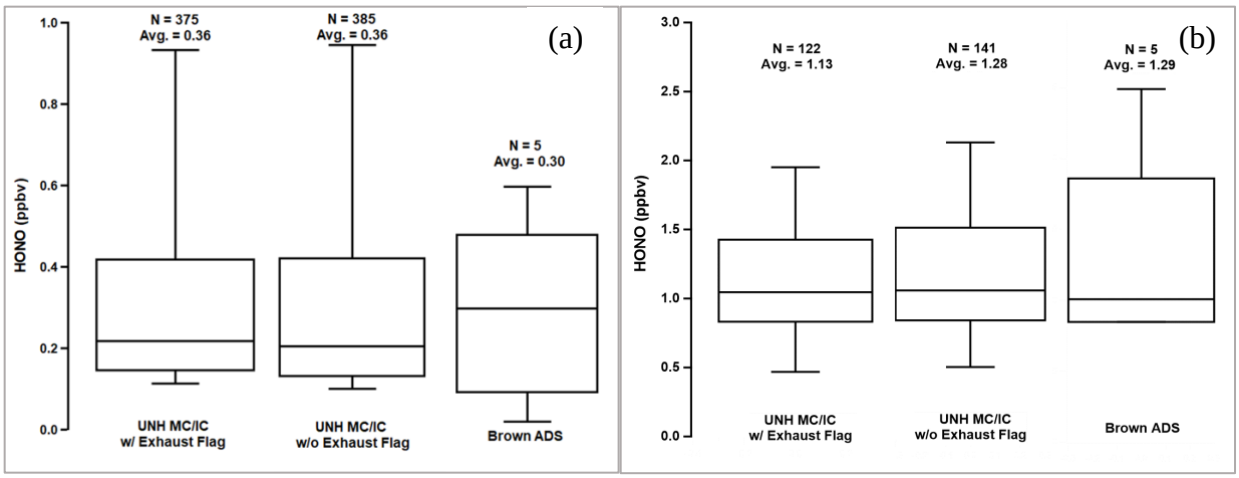

Figure S3. Comparison of HONO concentrations measured with MC/IC and that recovered from ADS collection for isotopic analysis for Williams Flats fire (a) and Nethker fire (b). The whiskers from bottom to top represent 10%, 25%, 50%, 75% and 90% quartiles.

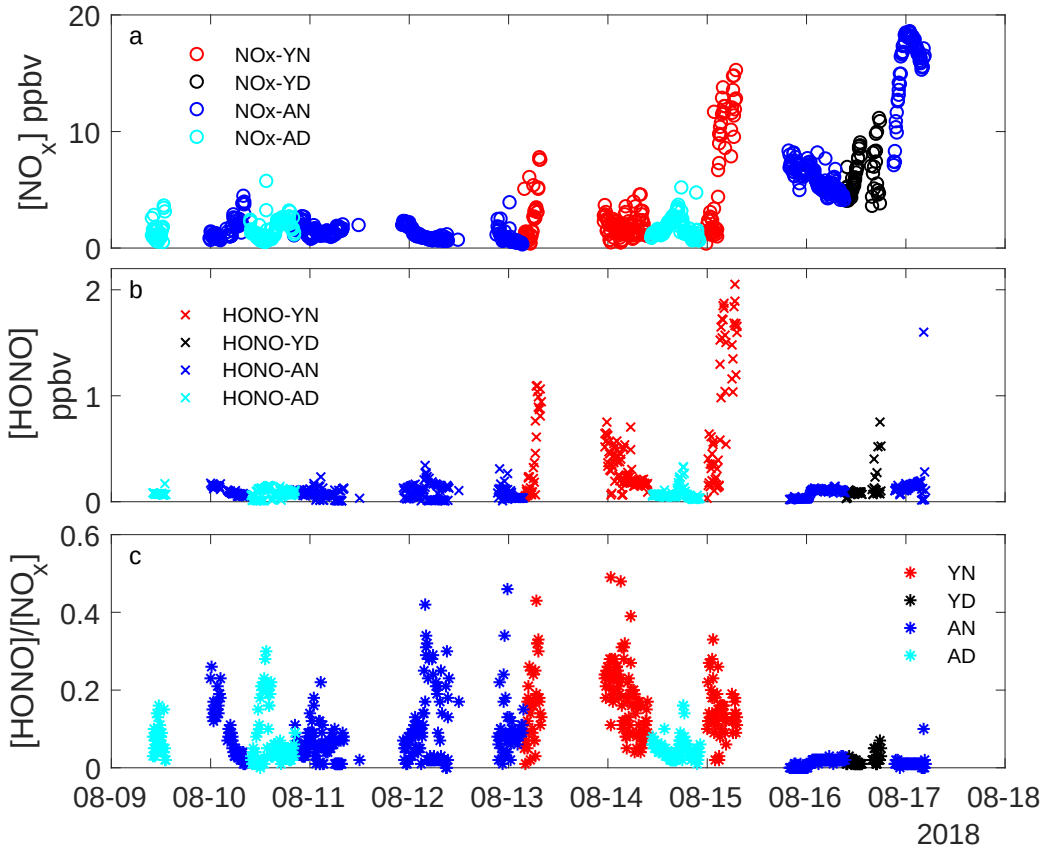

Figure S4. Time history of HONO/NO_x during WE-CAN 2018 sampling.

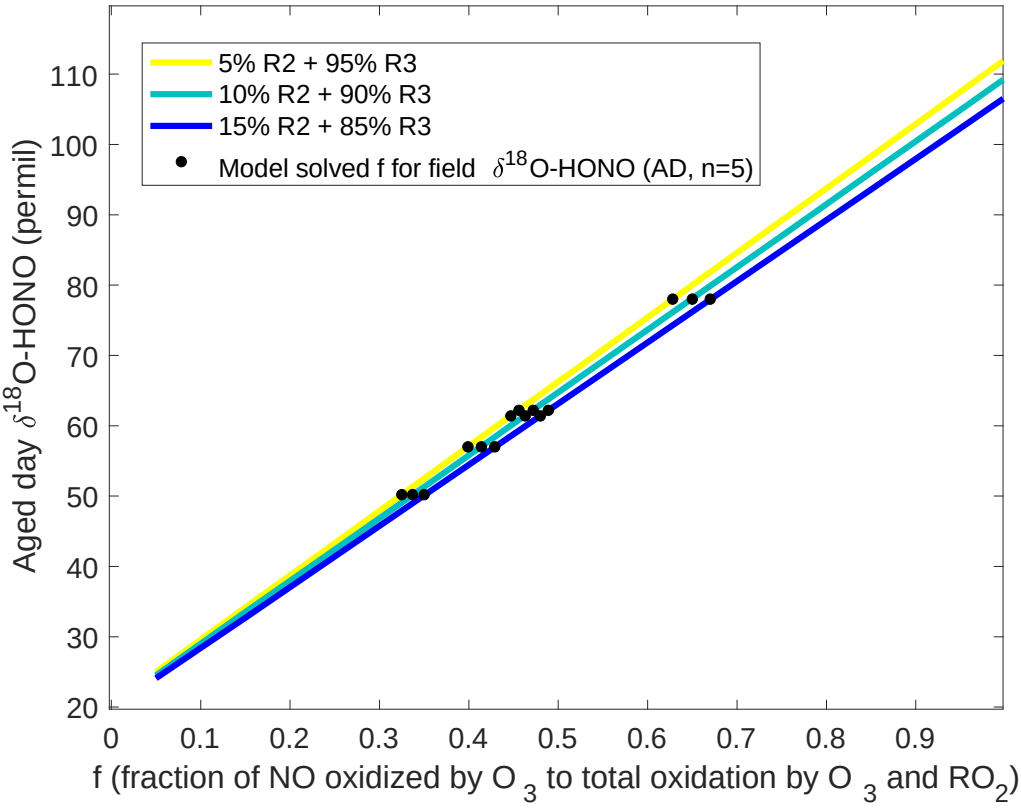

Figure S5. Modeling results for δ^{18}O-HONO in aged daytime smoke as a function of fraction of NO oxidized to NO_2 via O_3 to that via O_3 and RO_2 together ($f^{NO}_{O3/(O3+RO2)}$). The contribution of R2 to HONO production is varied from 5% to 15% following M1 in Fig. 4, and R3 accounts for the remaining secondary HONO contribution.

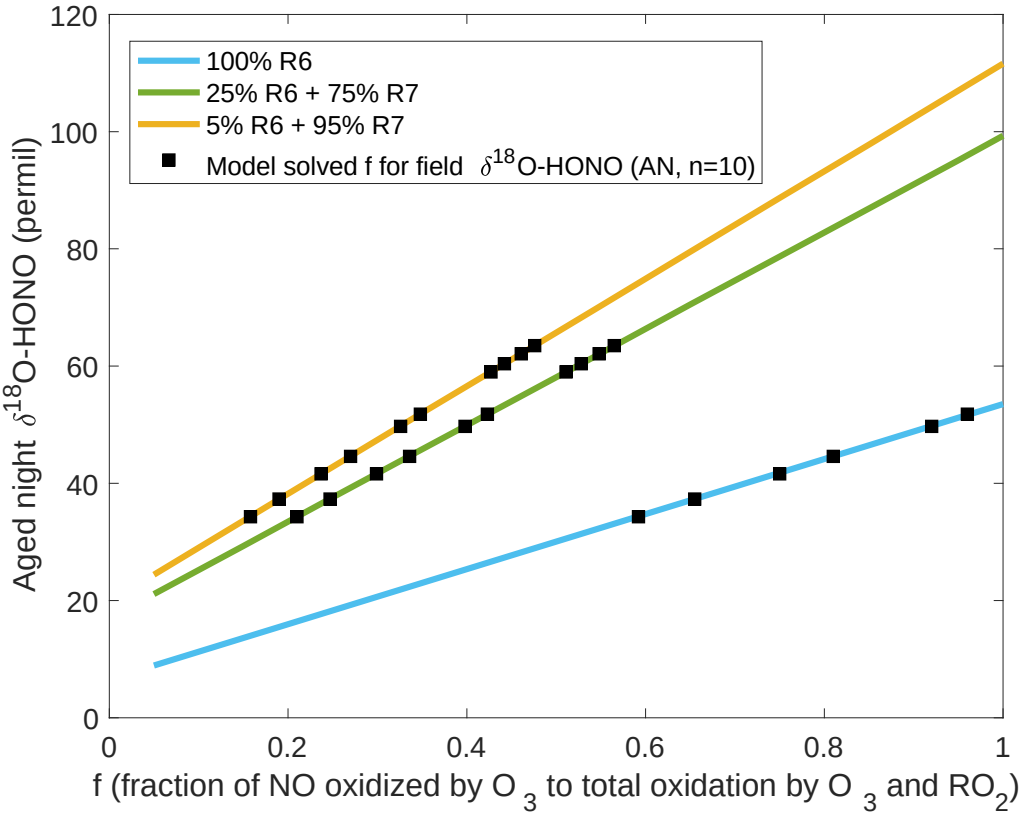

Figure S6. Modeling results for δ^{18}O-HONO in aged nighttime smoke as a function of fraction of NO oxidized to NO_2 via O_3 to that via O_3 and RO_2 together ($f^{NO}_{O3/(O3+RO2)}$). Three scenarios with various contributions of R6 and R7 are modeled. Black squares are model solved $f^{NO}_{O3/(O3+RO2)}$ to each field-observed δ^{18}O-HONO under this condition.

Table S1. Secondary formation and sink reactions and their isotopic enrichment factors for ^{15}N and ^{18}O ($^{15}\varepsilon$ and $^{18}\varepsilon$) estimated in this work.

Condition	Reaction	$^{15}\varepsilon$ ‰	$^{18}\varepsilon$ ‰
day	NO + OH —> HONO	+10	+15
day	HONO + hv —> NO + OH (λ<400 nm)	-2.5	-3.5
day	HONO + OH —> NO_2 + H_2O	N/A	N/A
day	HNO_3/NO_3^- + hv —>HONO + NOx	≤-47.9	6 to 13
day	organics + H_2O +NO_2 + hv	-2.9 to -4.5	-5.7 to -8.9
night	HONO (g) —> HONO (ads)	-2	-4
night	$2NO_2$ + H_2O —> HNO_3 + HONO	-2.9 to -4.5	-5.7 to -8.9
night	NO_2 + H_2O + Fe_xO_y (and/or quinone)	-2.9 to -4.5	-5.7 to -8.9

Table S2. Rate coefficients used in this work (Burkholder et al. 2019[a])

Reaction	Rate coefficient (298 K) $cm^3\ s^{-1}$
$HO_2 + NO \longrightarrow OH + NO_2$	8.0×10^{-12}
$NO + O_3 \longrightarrow NO_2 + O_2$	1.9×10^{-14}
$C_2H_5O_2 + NO \longrightarrow$ product	8.7×10^{-12}
$CH_3O_2 + NO \longrightarrow CH_3O + NO_2$	7.7×10^{-12}
$RO_2 + NO \longrightarrow$ product	8.0×10^{-12}
$RO_2 + NO \longrightarrow RONO_2$	3.2×10^{-13}

[a] Burkholder, J. B., Sander, S. P., Abbatt, J., Barker, J. R., Cappa, C., Crounse, J. D., Dibble, T. S., Huie, R. E., Kolb, C. E., Kurylo, M. J., Orkin, V. L., Percival, C. J., Wilmouth, D. M. and Wine P. H.: "Chemical Kinetics and Photochemical Data for Use in Atmospheric Studies, Evaluation No. 19," JPL Publication 19-5, Jet Propulsion Laboratory, Pasadena, 2019.

Table S3. Modeling results for $\Delta\delta^{15}N_{HONO\text{-}NOx}$ (‰).

Remaining HONO	$\Delta\delta^{15}N_{HONO\text{-}NOx}$ (5%R2+95%R3)	$\Delta\delta^{15}N_{HONO\text{-}NOx}$ (10%R2+90%R3)	$\Delta\delta^{15}N_{HONO\text{-}NOx}$ (15%R2+85%R3)	$\Delta\delta^{15}N_{HONO\text{-}NOx}$ (10%R2+85%R3 +5%R4)	$\Delta\delta^{15}N_{HONO\text{-}NOx}$ (10%R2+80%R3 +10%R4)	$\Delta\delta^{15}N_{HONO\text{-}NOx}$ (10%R2+75%R3 +15%R4)
0.9	-1.8	-1.2	-0.5	-3.4	-5.6	-7.8
0.8	-1.6	-0.9	-0.3	-3.1	-5.3	-7.5
0.7	-1.3	-0.6	0.0	-2.8	-5.0	-7.2
0.6	-0.9	-0.3	0.4	-2.5	-4.7	-6.9
0.5	-0.5	0.1	0.8	-2.1	-4.3	-6.5
0.4	0.0	0.7	1.3	-1.5	-3.7	-5.9
0.36	0.2	0.9	1.5	-1.3	-3.5	-5.7
0.32	0.5	1.2	1.8	-1.0	-3.2	-5.4
0.28	0.8	1.5	2.1	-0.7	-2.9	-5.1
0.24	1.2	1.8	2.5	-0.4	-2.6	-4.8
0.2	1.6	2.2	2.9	0.0	-2.2	-4.4
0.16	2.1	2.8	3.4	0.6	-1.6	-3.8
0.12	2.8	3.4	4.1	1.2	-1.0	-3.2
0.08	3.7	4.3	5.0	2.1	-0.1	-2.3
0.04	5.3	5.9	6.6	3.7	1.5	-0.7
0.02	6.8	7.5	8.1	5.3	3.1	0.9

Table S4. Modeling results for $\delta^{18}O$ aged daytime and aged nighttime (‰).

	Day			Night		
$k_{O3}[O_3]/$ $k_{RO2}[RO_2]+k_{O3}[O_3]$	$\delta^{18}O$-HONO (5%R2+ 95%R3)	$\delta^{18}O$-HONO (10%R2+ 90%R3)	$\delta^{18}O$-HONO (15%R2+ 95%R3)	$\delta^{18}O$-HONO (100%R6)	$\delta^{18}O$-HONO (25%R6+ 75%R7)	$\delta^{18}O$-HONO (5%R6+ 95%R7)
0.05	25.0	24.5	24.1	8.9	21.1	24.4
0.15	34.2	33.5	32.7	13.6	29.3	33.6
0.25	43.3	42.4	41.4	18.3	37.6	42.8
0.35	52.5	51.3	50.1	23.0	45.8	52.0
0.429	59.8	58.4	57.0	26.7	52.3	59.2
0.592	74.7	72.9	71.2	34.3	65.7	74.2
0.65	80.0	78.1	76.2	37.1	70.5	79.5
0.75	89.2	87.0	84.9	41.8	78.7	88.7
0.85	98.3	96.0	93.6	46.5	86.9	97.8
0.95	107.5	104.9	102.3	51.2	95.1	107.0
1	112.1	109.4	106.7	53.5	99.3	111.6